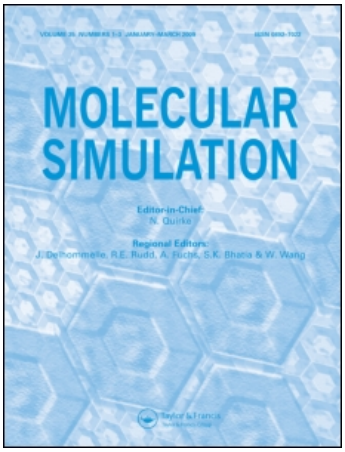

Molecular Simulation
Publication details, including instructions for authors and subscription information:
http://www.informaworld.com/smpp/title~content=t713644482

Excluded volume of hard cylinders of variable aspect ratio

N. Ibarra-Avalos[a]; A. Gil-Villegas[b]; A. Martinez Richa[a]
[a] Facultad de Química, Universidad de Guanajuato, Gto, México [b] Instituto de Física, Universidad de Guanajuato, León, México

To cite this Article Ibarra-Avalos, N. , Gil-Villegas, A. and Richa, A. Martinez(2007) 'Excluded volume of hard cylinders of variable aspect ratio', Molecular Simulation, 33: 6, 505 — 515
To link to this Article: DOI: 10.1080/08927020701191349
URL: http://dx.doi.org/10.1080/08927020701191349

Molecular Simulation, Vol. 33, No. 6, May 2007, 505–515

Taylor & Francis
Taylor & Francis Group

Excluded volume of hard cylinders of variable aspect ratio

N. IBARRA-AVALOS†¶, A. GIL-VILLEGAS‡* and A. MARTINEZ RICHA†§

†Facultad de Química, Universidad de Guanajuato, Noria Alta s/n, Guanajuato, Gto 36050, México
‡Instituto de Física, Universidad de Guanajuato, Lomas del Bosque 103, Colonia Lomas del Campestre, León 37150, México

(Received October 2006; in final form January 2007)

In this article, we report expressions for the excluded volume, v_{ex} and second virial coefficient, B_2, of hard cylinders as a function of their aspect ratio ($\mathcal{A} = L/D$), where L and D are the length and diameter of the cylinder, respectively. These expressions are valid for aspect ratio values within the interval $0.001 < \mathcal{A} < 100$, that covers from thin plates to long rods and reproduce Monte Carlo (MC) simulation values. We compare these results with Onsager's predictions and with reported values of hard bodies of similar geometry, as cut spheres (CS), hard spherocylinders (HSC) and linear tangent hard sphere chains (LTHSC). Simulation values for v_{ex} were obtained with an overlap algorithm that is also presented in detail. The obtained results can be applied in theoretical and computer simulation studies of discotic liquid crystals.

Keywords: Hard bodies; Excluded volume; Monte Carlo simulations; Discotic liquid crystals

1. Introduction

The modeling of molecules by hard bodies plays a key role in statistical theories and has proved to be a useful tool to gain a better understanding of the relation between the macroscopic and microscopic properties of simple and complex fluids [1–4]. In the case of liquid crystalline materials fundamental questions about the factors that determine the formation of mesophases have been answered theoretically and by computer simulations using very simple model systems. Among other things, we know that the spatial exclusion due to harsh repulsive forces is the dominant factor in determining the fluid structure and that a variety of liquid crystalline phases can be induced by steric forces [5–10]. The understanding of the macroscopic properties on a molecular level demands the knowledge of molecular interaction parameters. Real mesogens present molecular features such as flexible tails and anisotropic forces that are not essential for mesophase formation, but they are the fine details that determine its phase behaviour [11–18].

When a hard core shape is chosen for modeling a molecular fluid, it is important to take into account the degree of approximation introduced by the shape of the hard core, the required number of geometric parameters and the procedure to be used to determine whether or not two cores overlap [19]. Moreover, a hard core model for which is possible to calculate analytically its excluded volume, v_{ex}, for a pair of molecules at an arbitrary orientation, offers an extra advantage for the theoretical prediction of the phase properties of the model system.

In this paper, we study the excluded volume of hard cylinders of variable aspect ratio $\mathcal{A} = L/\sigma$, where L is the length and σ the diameter of the particles. In section 2, two different methods are used to determine the excluded volume: (a) Monte Carlo (MC) simulations based on an overlap algorithm for hard cylinders and (b) a semi-analytical calculation. Closed expressiones are given for v_{ex} that are valid for the whole range of aspect ratios values, that covers from very thin plates to very long rods. Our approach is compared with Onsager's results [5] and the second virial coefficient is also determined. In section 3, a detailed description of the semianalytical derivation of the excluded volume is presented and in Section 4, the conclusions to this work are given. In the appendix, we present a detailed description of the overlap algorithm used in this study.

*Corresponding author. Email: gil@fisica.ugto.mx
¶Email: niza_ibarra@yahoo.com
§Email: richa@quijote.ugto.mx

Molecular Simulation
ISSN 0892-7022 print/ISSN 1029-0435 online © 2007 Taylor & Francis
http://www.tandf.co.uk/journals
DOI: 10.1080/08927020701191349

2. Excluded volume

According to Onsager [5], the excluded volume for a pair of cylinders of lengths L_1 and L_2, diameter σ and relative orientation γ is given by

$$v_{ex}(L_1, L_2, \sigma, \gamma) = \frac{\pi}{4}(L_1 + L_2)\sigma^2 + \frac{\pi}{2}\sigma^3 \sin\gamma + 2L_1L_2\sigma\sin\gamma + \frac{\pi}{4}(L_1 + L_2)\sigma^2|\cos\gamma| + (L_1 + L_2)\sigma^2 E(\sin\gamma) \quad (1)$$

where $E(\sin\gamma)$ denotes the elliptic integral of the second kind,

$$E(\sin\gamma) = \int_0^{\pi/2} \left(1 - \sin^2\gamma\sin^2\phi\right)^{1/2} d\phi.$$

We can also study numerically the same quantity using a computer simulation scheme. Through a MC procedure, the excluded volume is obtained as

$$v_{ex}(\gamma) = \lim_{N_{tot}\to\infty} \frac{N_{ov}(\gamma)}{N_{tot}(\gamma)} V \quad (2)$$

where $N_{tot}(\gamma)$ is the total number of configurations generated for the pair of cylinders with arbitrary positions and relative orientation γ, $N_{ov}(\gamma)$ is the number of overlaping configurations and V is the volume of the sampling space. To sample the configurations, we need an overlap algorithm.

The overlap test for a pair of hard cylinders has been outlined [4] and a scheme for its implementation has been discussed by Blaak *et al.* [20]. We have followed a scheme that is a variation from the previous ones. The problem is analyzed by a sequence of elementary tests, namely

(a) Overlap test of two disk surfaces;
(b) overlap test of a cylindrical rim and a disk surface; and
(c) overlap test of two cylindrical rims.

These overlap tests are sufficient to determine any possible overlap configuration between a pair of hard cylinders, independently of the value of the aspect ratio $\mathcal{A}$. The overlap configurations described by the elementary tests given previously are ilustrated in figure 1 for a pair of hard cylinders with aspect ratio $\mathcal{A} = 1$. A detailed description of the overlap algorithm is given in the Appendix, that can be implemented directly in a computer code.

Using this scheme, implemented through the procedures described in the Appendix, MC simulations were performed to obtain the excluded volume $v_{ex}(\gamma)$ of three different systems: (a) a pair of disks, (b) a disk and a cylinder and (c) a pair of cylinders. Simulations were done with $N_{tot} = 1000$ millions of configurations and considering that the orientation of one of the molecules is along the z-axis, so that γ corresponds to the polar angle. The volume of the sampling space, V, is a cube centered in a fixed particle. This particle is aligned along the z-axis. The configurations of a second particle moving around the fixed particle are obtained by a uniform random sampling within the cube.

In figure 2, we compare the simulated results for the excluded volume of a pair of disks of diameter σ and

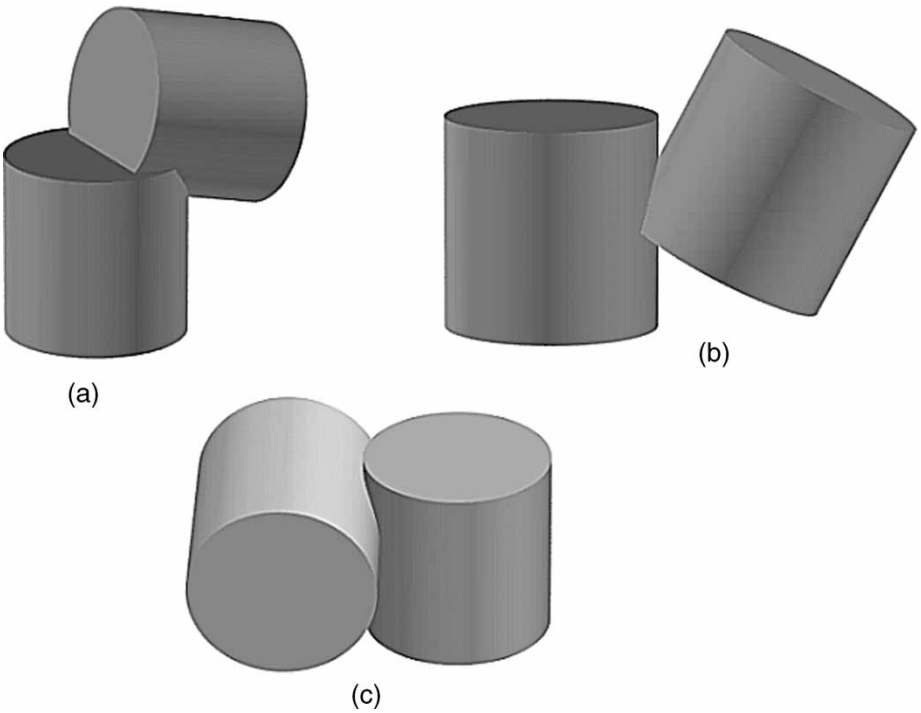

Figure 1. Snapshots of overlap configurations for a pair of cylinders with aspect ratio $\mathcal{A} = 1$: (a) disk–disk, (b) disk–cylindrical rim and (c) cylindrical rim–cylindrical rim overlaps. These are the three different overlap configurations that are neccesary to describe any overlap configuration.

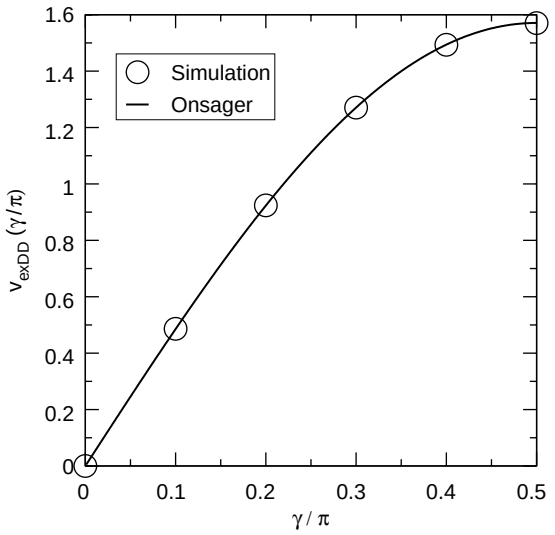

Figure 2. Excluded volume for a pair of disks of diameter σ as a function of their relative orientation γ, expressed in units of σ^3. MC results (open circles) are compared with Onsager theory (solid line).

relative orientation γ, $v_{ex_{DD}}(\sigma, \gamma)$, compared with the Onsager's expression, equation (1) with $L_1 = L_2 = 0$. The agreement between simulation and theory is within four significative figures.

In figure 3 (a) and (b), we report the comparison between MC values and Onsager's predictions for the excluded volume of a disk and a cylinder with the same diameter σ. In this case, we apply equation (1) with $L_2 = 0$. Results are reported for different cylinder's aspect ratios, $\mathcal{A}$. The excluded volume $b_{CD}(\mathcal{A},\gamma)$, is given in terms of the cylinder volume,

$$b_{CD}(\mathcal{A}, \gamma) = \frac{v_{ex_{CD}}(\mathcal{A}, \gamma)}{v_{cil}} = \frac{v_{ex_{CD}}(\mathcal{A}, \gamma)}{\frac{\pi}{4}\mathcal{A}\sigma^3}.$$

A deviation of the order of 0–5% between simulated and Onsager results is obtained in this case and we found that the largest deviation happens around, $\gamma = \pi/4$, for intermediate values of the aspect ratio.

In order to have a better understanding of the deviations observed between MC values and the Onsager theory's predictions, we calculated the excluded volume, following Onsager's original derivation [5]. The excluded volume for a disk–cylinder system can be expressed as

$$v_{ex_{CD}}(\mathcal{A}, \sigma, \gamma) = \frac{\pi}{4}\sigma^3 \sin\gamma + \mathcal{S}_{\perp}(\sigma, \gamma)L,$$

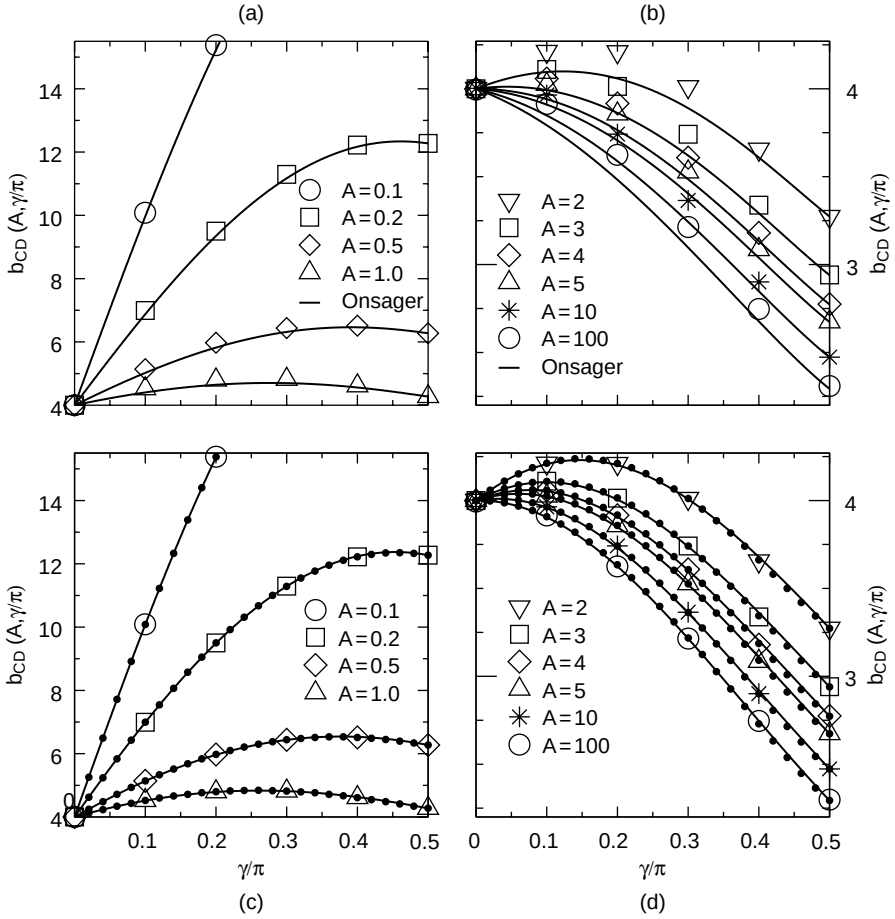

Figure 3. Excluded volume for a disk moving around a hard cylinder. In (a) and (c), the cylinder is oblate, ($\mathcal{A} \leq 1$) and in (b) and (d) is prolate, ($\mathcal{A} > 1$). In (a) and (b), MC results (open symbols) are compared with Onsager theory's predictions (solid lines) for several values of the aspect ratio $\mathcal{A}$. In (c) and (d), the same simulation results are compared with the semianalytical results (solid line) and the parametric expression given by equation (4) (dot lines).

or, in terms of the volume of the cylinder, v_{cil},

$$b_{CD}(\mathcal{A}, \sigma, \gamma) = \frac{2}{\mathcal{A}}\sin\gamma + \frac{4}{\pi\sigma^2}\mathcal{S}_{\perp}(\sigma, \gamma), \qquad (3)$$

where $\mathcal{S}_{\perp}(\sigma,\gamma)$, in units of σ^2, is the area projected by the excluded volume $v_{ex_{CD}}(\sigma, \gamma)$ onto a perpendicular plane to the disk's axis. According to Onsager, $\mathcal{S}_{\perp}$ is delimited by the center of a circle that rolls over an ellipse and applies a method for rolling-figures of continuous tangent to evaluate it. See figures 3 and 4 from the Appendix in Ref. [5]. However, as we describe in Section 3, we obtained $\mathcal{S}_{\perp}$ as the envelope of a family of semiellipses centered in a circumference. Although in this case, it is not possible to obtain the excluded volume as a closed expression as in Onsager's theory, equation (1), the numerical results are in excellent agreement with the MC values and have the same deviation as the simulated values with respect to Onsager theory's results. This comparison is reported in figure 3(c) and (d). In table 1, we present a comparison of excluded volumes of two different disk–cylinder systems, obtained by the three methods already discussed: Onsager's theory, MC simulations and semianalytical procedure. In these reported systems, the cylinders correspond to aspect ratios $\mathcal{A} = 2$ and 3. The deviations observed between the Onsager results and the values obtained with the other two methods are not within the statistical uncertainty. Also in this table, we present a comparison of two different ways of choosing the sampling volume in equation (2), a cube or a sphere, in the MC calculations. As we can see from this comparison, the shape of the sampling volume is no relevant for the final equilibrated results.

It is important to stress here that function $\mathcal{S}_{\perp}(\sigma,\gamma)$ is obtained numerically. However, a simple parameteric representation has been found to reproduce very accurately equation (3) and the MC simulated values,

$$b_{CD}(\mathcal{A}, \gamma) = 1 + \frac{4}{\pi} + \frac{2}{\mathcal{A}}\sin\gamma + \left(\frac{3\pi}{4} - 1\right)|\cos\gamma| + \left(3 - \frac{4}{\pi}\right)\left(1 - \frac{\pi}{4}\right)\cos^2\gamma. \qquad (4)$$

Results of this parametric formula are presented in figure 3(c) and (d). As we can see, there is agreement between Onsager's theory, MC values and the parametric formula given before, for the limits $\mathcal{A} \ll 1$ and $\mathcal{A} \gg 1$. In order to compare directly equation (4) with Onsager's expression, we fix $L_2 = 0$, $\mathcal{A} = L_1/\sigma$ and reduce equation (1) by v_{cil}, obtaining

$$b_{CD}^{Onsager}(\mathcal{A}, \gamma) = 1 + \frac{2}{\mathcal{A}}\sin\gamma + |\cos\gamma| + \frac{4}{\pi}E(\sin\gamma). \qquad (5)$$

Both expressions have the same dependency on $\sin\gamma$, term that comes from the excluded volume of a pair of disks, see next section. Expression (4) is a simple formula that agrees with simulated results; the major observed deviation is for $b_{CD}(5,(2/5)\pi)$ and is less than 0.7%.

For the case of the excluded volume of a pair of identical cylinders, $b_{CC}(\mathcal{A},\gamma)$, we found that the deviation between MC and Onsager's values is within the range 0–3.1% and the largest deviation corresponds to $b_{CC}(1,(1/5)\pi)$. See figure 4.

Table 1. Reduced excluded volume b_{CD} and statistical errors for the systems cylinder–disk of aspect ratios $\mathcal{A} = 2$ and 3. The MC results obtained for two different sampling volumes are shown in comparison with Onsager's expression, equation (5) and equation (3) with $\mathcal{S}_{\perp}(\sigma,\gamma)$ evaluated numerically as explained in Section 3. The uncertainty of the last two digits is represented in parentheses.

		b_{CD}				
$\mathcal{A}$	γ/π	*Onsager*	*Semianalytical*	*Squared box 10^9 configurations*	*Squared box 10^{10} configurations*	*Spherical box 10^9 configurations*
2	0.00	4.00000	4.00000	4.0006(06)	4.0002(03)	4.0002(01)
	0.05	4.06345	4.13183	4.1319(08)	4.1318(05)	4.1321(02)
	0.10	4.09522	4.21143	4.2115(13)	4.2112(04)	4.2114(02)
	0.15	4.09373	4.23757	4.2376(09)	4.2373(04)	4.2378(01)
	0.20	4.05841	4.21086	4.2110(10)	4.2109(04)	4.2105(02)
	0.25	3.98975	4.13390	4.1342(09)	4.1339(05)	4.1339(03)
	0.30	3.88951	4.01145	4.0115(10)	4.0115(04)	4.0110(02)
	0.35	3.76090	3.85071	3.8508(33)	3.8504(03)	3.8509(02)
	0.40	3.60900	3.66199	3.6617(35)	3.6620(06)	3.6619(01)
	0.45	3.44163	3.46038	3.4600(24)	3.4603(02)	3.4605(02)
	0.50	3.27324	3.27324	3.2733(08)	3.2733(05)	3.2733(01)
3	0.00	4.00000	4.00000	4.0001(11)	4.0000(04)	4.0001(02)
	0.05	4.01130	4.07968	4.0799(08)	4.0797(05)	4.0795(04)
	0.10	3.99221	4.10843	4.1085(15)	4.1083(04)	4.1085(02)
	0.15	3.94240	4.08624	4.0863(12)	4.0860(07)	4.0862(02)
	0.20	3.86248	4.01493	4.0145(10)	4.0149(06)	4.0146(02)
	0.25	3.75405	3.89820	3.8982(12)	3.8982(07)	3.8984(03)
	0.30	3.61984	3.74178	3.7420(19)	3.7419(04)	3.7415(02)
	0.35	3.46390	3.55371	3.5538(09)	3.5536(03)	3.5540(03)
	0.40	3.29198	3.34497	3.3448(10)	3.3451(06)	3.3449(03)
	0.45	3.11240	3.13115	3.1308(08)	3.1314(04)	3.1314(02)
	0.50	2.93991	2.93991	2.9398(09)	2.9399(06)	2.9401(02)

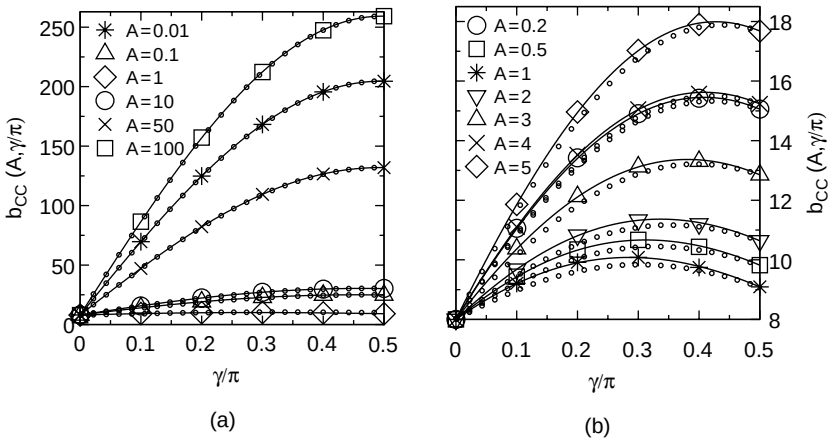

Figure 4. Excluded volume for a pair of cylinders with different aspect ratios $\mathcal{A}$ and for different relative orientations γ. MC results (symbols) are compared with Onsager theory (dots) and the parametric expression given by equation (6) (solid line). Extreme and intermediate values of $\mathcal{A}$ are shown in (a) and (b), respectively.

A simple modification of equation (4) gives an excellent parametric representation of $b_{CC}(\mathcal{A},\gamma)$,

$$b_{CC}(\mathcal{A},\gamma) = 2 + \frac{8}{\pi} + \left(\frac{2}{\mathcal{A}} + \frac{8}{\pi}\mathcal{A}\right)\sin\gamma + 2\left[\left(\frac{3\pi}{4} - 1\right)|\cos\gamma| + \left(3 - \frac{4}{\pi}\right)\left(1 - \frac{\pi}{4}\right)\cos^2\gamma\right]. \quad (6)$$

The corresponding Onsager's expression is obtained using $L_1 = L_2 = L$, $\mathcal{A} = L/\sigma$ in equation (1) and scaling with respect to v_{cil},

$$b_{CC}^{Onsager}(\mathcal{A},\gamma) = 2 + \left(\frac{2}{\mathcal{A}} + \frac{8}{\pi}\mathcal{A}\right)\sin\gamma + 2|\cos\gamma| + \frac{8}{\pi}E(\sin\gamma).$$

In figure 4, we report the comparison between both expressions. The largest deviation of equation (6) and the MC data corresponds to $b_{CC}(2,(2/5)\pi)$ and is less than 0.4%.

As a direct application of previous results, the second virial coefficient $\mathcal{B}_2$ for an isotropic phase has been calculated from equation (6) and the relation

$$\mathcal{B}_2 = \frac{1}{2}\langle v_{exc}\rangle \quad (7)$$

obtaining

$$\mathcal{B}_2(\mathcal{A}) = \frac{11}{6} + \frac{8}{3\pi} + \frac{\pi}{8} + \mathcal{A} + \frac{\pi}{4\mathcal{A}}. \quad (8)$$

In table 2, we present the results for the second virial coefficients of oblate and prolate hard cylinder molecules for an isotropic phase, in comparison with values of $\mathcal{B}_2$ given by Onsager [5], which, reduced with respect to the volume of a cylinder, can be written as

$$\mathcal{B}_2(\mathcal{A}) = \frac{3+\pi}{2} + \mathcal{A} + \frac{\pi}{4\mathcal{A}}. \quad (9)$$

The difference between the parametric formula and Onsager's result is a constant value equal to 0.00406. In the same table, we also report simulated values for cut spheres (CS) [21], hard spherocylinders (HSC) [22] and linear tangent hard spheres (LTHSC) [23]. The behaviour of $\mathcal{B}_2$ as a function of $\mathcal{A}$ is presented in figure 5(a) and (b). In (a), we can observe that the parametric expression developed here agrees with the Onsager prediction. Notice that the differences previously observed for the Onsager and simulated and parametric excluded volumes are not large enough in order to make a significant deviation between the corresponding second virial coefficients. In (b), this parametric expression is compared with the values for

Table 2. MC values for the second virial coefficient $\mathcal{B}_2$ of hard cylinders for several aspect ratios $\mathcal{A}$. Results are compared with values of $\mathcal{B}_2$ for CS [21], HSC [3,22] and LTHSC [23]. Onsager's theory predictions for hard cylinders are also included [5].

$\mathcal{A}$	$\mathcal{B}_2$	$\mathcal{B}_2^{Onsager}$	$\mathcal{B}_2^{CS}$	$\mathcal{B}_2^{HSC}$	$\mathcal{B}_2^{LTHSC}$
0.001	788.5	788.5			
0.01	81.62	81.62			
0.1	11.03	11.02	11.27		
0.2	7.202	7.198	7.402		
0.3	5.993	5.989	6.133		
0.4	5.438	5.434			
0.5	5.146	5.142			
1.0	4.860	4.856	4.000	4.600	4.000
2.0	5.468	5.463		5.500	5.444
3.0	6.337	6.333		6.455	6.850
4.0	7.271	7.267		7.429	8.248
5.0	8.232	8.228		8.412	9.641
6.0	9.206	9.202		9.400	11.03
7.0	10.19	10.18		10.39	12.42
8.0	11.17	11.17		11.38	13.81
9.0	12.16	12.16		12.38	15.20
10	13.15	13.15		13.38	16.59
50	53.09	53.09		72.11	72.11
100	103.1	103.1		103.3	141.5

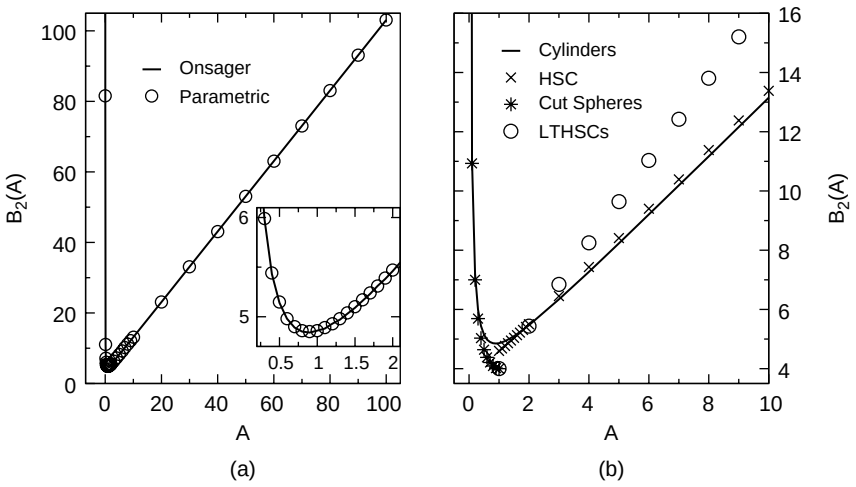

Figure 5. (a) Second virial coefficient for hard cylinders for aspect ratios $0.01 \leq \mathcal{A} \leq 100.0$ as predicted by equation (8) (solid line) and compared with Onsager values given by equation (9) (circles). (b) Results are compared with systems of similar geometry: CS (stars) [21], HSC (crosses) [3,22] and LTHSC (circles) [23].

systems of similar geometry. It can be observed that $\mathcal{B}_2$ for hard cylinders and thin cut-spheres systems have very similar values. On the other hand, for aspect ratios $\mathcal{A} > 1$, the hard cylinders and the LTHSC systems have strong deviations. This figure also illustrates how $\mathcal{B}_2$ evolves as the geometry of the systems changes from LTHSC to hard cylinders. By increasing $\mathcal{A}$, HSC and hard cylinders tend to exclude the same volume. This effect can be seen in Table 2, where for $\mathcal{A} = 100$ both systems have almost the same value of $\mathcal{B}_2$. On the other hand, the LTHSC values of $\mathcal{B}_2$ are higher than the HSC and hard cylinders values as $\mathcal{A}$ increases, since the second virial coefficient is scaled with the volume of a particle. This means that as $\mathcal{A}$ increases, the volume of a LTHSC system is lower than the volume of a HSC or a hard cylinder. The observed effect is then a consequence of the non-convex shape of the LTHSC particle.

3. Semianalytical calculation of the excluded volume of disk–disk and disk–cylinder systems

In this section, we present a semianalytical derivation of the excluded volume of hard cylinders whose main results were presented in the previous section. We study specifically the disk–disk and disk–cylinder systems, because these systems allow us to understand the deviations observed with respect to Onsager theory. The case of the disk–disk system is analytical and reproduces Onsager's expression, whereas in the case disk–cylinder is not possible to obtain a closed expression as Onsager did. However, as we have discussed in Section 2, the results obtained in this work reproduce the MC simulated values.

3.1 Excluded volume for a pair of disks

We denote by $v_{\mathrm{ex_{DD}}}(\sigma_1, \sigma_2, \gamma)$ the excluded volume of a pair of disks of diameters σ_1 and σ_2. The center of the disk 1 is located at the origin with its normal oriented along the z-axis. Disk 2 moves around disk 1 with the restriction that the relative orientation γ between disks is kept fixed. By definition $v_{\mathrm{ex_{DD}}}(\sigma_1, \sigma_2, \gamma)$ is the inaccessible volume to disk 2.

Let us consider figure 6, that depicts the excluded volume element that disk 2 generates when rolls over the chord AB perpendicular to the x-axis. This volume is determined by the length of chord AB and the diameter σ_2, independently of the relative orientation γ. See diagrams (a) and (b). The area inside the contour is given by the area of the rectangle of sides $|\mathbf{A} - \mathbf{B}|$ and σ_2, added to the area of the semicircles of diameter σ_2, as shown in diagram (c). The excluded volume of this system is given by the sum of all the volume elements generated by all the chords of disk 1 that are perpendicular to the x-axis. To clarify this point, in figure 7, we show two representations of the excluded volumes $v_{\mathrm{ex_{DD}}}(\sigma, \sigma/2, \pi/2)$ and $v_{\mathrm{ex_{DD}}}(\sigma, \sigma/2, 7\pi/18)$. By construction, every volume element can be decomposed into rectangular and semicircular components, as shown

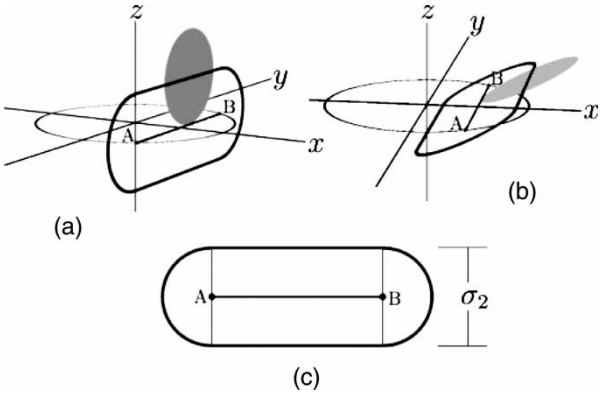

Figure 6. Contours of the volume element obtained by a disk rolling on a chord AB of other disk with center in the origin and normal (0,0,1), as explained in the text. The contour depends only on the length of chord AB and is independent of the relative orientation γ between disks.

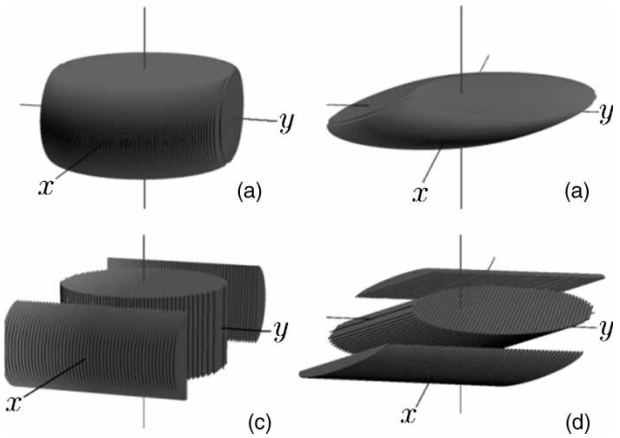

Figure 7. Approximated representations of the excluded volumes (a) $v_{ex_{DD}}(\sigma, \sigma/2, \pi/2)$ and (b) $v_{ex_{DD}}(\sigma, \sigma/2, 7\pi/18)$. The same volumes are equivalently described in (c) and (d) by separating the rectangular and semicircle components of the excluded volume elements, as explained in the text.

in this figure. Therefore the volume shown in (a) is equivalent to the volume (c) and the volume in (b) is equivalent to the volume in (d). It is clear then that $v_{ex_{DD}}(\sigma_1, \sigma_2, \gamma)$ is given by the sum of the volume of two oblique cylinders with transverse section areas $(\pi/4)\sigma_1^2$ and $(\pi/4)\sigma_2^2 \sin\gamma$ and heights $\sigma_2 \sin\gamma$ and σ_1, respectively. The final expression obtained is

$$v_{ex_{DD}}(\sigma_1, \sigma_2, \gamma) = \left(\frac{\pi}{4}\sigma_1^2\right)(\sigma_2 \sin\gamma) + \left(\frac{\pi}{4}\sigma_2^2 \sin\gamma\right)(\sigma_1) = \frac{\pi}{4}\sigma_1\sigma_2(\sigma_1 + \sigma_2)\sin\gamma. \quad (10)$$

which agrees with the expression derived by Onsager in the Appendix of Ref. [5].

3.2 Excluded volume for a cylinder and a disk

We consider now the excluded volume when we have a disk of diameter σ_2 moving around a fixed cylinder with diameter σ_1 and length L, i.e. its aspect ratio is $\mathcal{A} = L/\sigma_1$.

The cylinder is oriented along the z-axis, in such a way that its caps are located at $z = 0$ and L. The relative orientation between the disk and the cylinder is γ. We assume now that the cylinder can be generated by an infinite superposition of disks regularly spaced between the caps of the cylinder. The disk located at the bottom ($z = 0$) will exclude a volume given by equation (10) and we will denote it as $v_{ex_{DD0}}$. If we consider the cylinder next to this one, then it will exclude a volume $v_{ex_{DD1}}$ that will be the same as $v_{ex_{DD0}}$, but displaced by a distance dz from the origin in the direction (0,0,1), being (0,0,dz) the vector position of the center of the second disk. In general form, $v_{ex_{DDn}}$ is the excluded volume by the n-th disk of the cylinder and is the same as $v_{ex_{DD0}}$ displaced a distance $n\,$dz in the direction (0,0,1). By considering all these excluded volumes together, we have that the excluded volume for this cylinder–disk system can be written as

$$v_{ex_{CD}}(\mathcal{A}, \sigma_2, \gamma) = \bigcup_n v_{ex_{DDn}}(\sigma_1, \sigma_2, \gamma).$$

The volume generated by adding $v_{ex_{DDn}}(\sigma_1, \sigma_2, \gamma)$ according to this expression is equivalent to the volume described by the translation of $v_{ex_{DD0}}(\sigma_1, \sigma_2, \gamma)$ from $z = 0$ to L, i.e.

$$v_{ex_{CD}}(\mathcal{A}, \sigma_2, \gamma) = v_{ex_{DD1}}(\sigma_1, \sigma_2, \gamma) + \mathcal{S}_\perp L, \quad (11)$$

where $\mathcal{S}_\perp = \mathcal{S}_\perp(\sigma_1,\sigma_2,\gamma)$ is the area of the projection of $v_{ex_{DD0}}(\sigma_1, \sigma_2, \gamma)$ onto the xy-plane, i.e. the plane defined by the normal (0,0,1). Since this projection is symmetric with respect to the xz- and yz-planes, as is shown in figure 6, then

$$\mathcal{S}_\perp(\sigma_1, \sigma_2, \gamma) = 4\int_0^{x_{max}(\gamma)} y_c(\sigma_1, \sigma_2, \gamma, x)\,dx. \quad (12)$$

where $y_c(\sigma_1,\sigma_2,\gamma,x)$ is a function that describes the contour of $\mathcal{S}_\perp(\sigma_1,\sigma_2,\gamma)$ within the quadrant ($0 < x, 0 < y$). As we shall probe later, $x_{max}(\gamma) = (\sigma_1 + \sigma_2 \cos\gamma)/2$.

In order to determine y_c, we consider that $v_{ex_{DD}}$ is generated by the excluded volume elements depicted in figures 6 and 7. In this way, $\mathcal{S}_\perp$ is given by the union of the projections onto the xy-plane of these excluded volume elements. Let us consider the set of semicircles with centers $\mathbf{B} = (x_B, y_B) = (x_B, \sqrt{(\sigma_1/2)^2 - x_B^2})$ belonging to the excluded volume elements depicted in these figures. The projection on the xy-plane of this set of semicircles can be described by a family $\mathcal{F}$ of semiellipses, each one defined by the equation

$$y_s(\sigma_1, \sigma_2, \gamma, x_B, x) = y_B + \sqrt{\left(\frac{\sigma_2}{2}\right)^2 - \left(\frac{x - x_B}{\cos\gamma}\right)^2} = \sqrt{\left(\frac{\sigma_1}{2}\right)^2 - x_B^2} + \sqrt{\left(\frac{\sigma_2}{2}\right)^2 - \left(\frac{x - x_B}{\cos\gamma}\right)^2}, \quad (13)$$

where parameter x_B, denoting the abscissa of the center of the ellipse, takes values within the interval $[0,\sigma_1/2]$. To clarify this point, we present in figure 8 the projections onto the xy-plane of three sets of circles with centers $\mathbf{B} = (x_B, \sqrt{(\sigma_1/2)^2 - x_B^2})$, radius $\sigma_2 = \sigma_1/2$ and relative orientations $\gamma = \pi/2, 7\pi/18$ and 0. In this figure, the upper semieplipses are described by equation (13).

With exception of the case $\gamma = \pi/2$, the family of semiellipses described by equation (13) has an envelope described by $y_c(\sigma_1,\sigma_2,\gamma,x)$. A common procedure to determine the envelope is to eliminate x_B from the

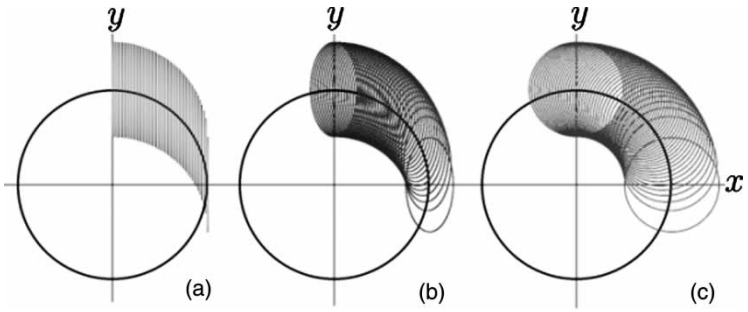

Figure 8. Projections onto the xy-plane of three different sets of circles with centers $\mathbf{B} = (x_B, \sqrt{(\sigma_1/2)^2 - x_B^2})$ and radius $\sigma_2 = \sigma_1/2$. In (a), the circles have a relative orientation $\gamma = \pi/2$ with respect to the z-axis, whereas in (b) and (c), $\gamma = 7\pi/18$ and 0, respectively.

following pair of equations

$$f(y, x_B, x) = 0$$

$$\frac{\partial}{\partial x_B} f(y, x_B, x) = 0$$

where

$$f(y, x_B, x) = y - \sqrt{\left(\sigma_1/2\right)^2 - x_B^2} - \frac{1}{2\cos\gamma}\left[\sigma_2^2 \cos^2\gamma - 4(x - x_B)^2\right]^{1/2}.$$

However, an easier procedure is to evaluate numerically $y_c(\sigma_1,\sigma_2,\gamma,x)$, as we discuss now.

Every one of the points $\mathbf{B} = (x_B,y_B)$ that belongs to the circumference $y_B(x_B) = \sqrt{(\sigma_1/2)^2 - x_B^2}$ will generate a unique semiellipse $y_s(\sigma_1,\sigma_2,\gamma,x_B,x)$ from the family $\mathcal{F}$. Since $y_c(\sigma_1,\sigma_2,\gamma,x)$ is the envelope of $\mathcal{F}$, each semiellipse y_s contributes to y_c with only one contact point. There is a biunivoc mapping between the points $\mathbf{B}$ and the points that belong to y_c. Given a point $\mathbf{B} = (x_B,y_B(x_B))$, we can calculate the point mapped onto the curve $y_c(\sigma_1,\sigma_2,\gamma,x)$ by a corresponding point from the semiellipse $y_s(\sigma_1,\sigma_2,\gamma,x_B,$-$_s(\sigma_1,\sigma_2,\gamma,x_B,x)$, generated by $\mathbf{B}$. This point is given by

$$(x_c, y_s(\sigma_1, \sigma_2, \gamma, x, x_c)), \tag{14}$$

where

$$x_c(\sigma_1, \sigma_2, \gamma, x_B) = x_B\left\{1 + \frac{\sigma_2 \cos^2\gamma}{\left(\sigma_1^2 - 4x_B^2 \sin^2\gamma\right)^{1/2}}\right\} \tag{15}$$

is obtained from the condition that curves y_s and y_c have the same tangent at their contact point. In the limit $\mathcal{N} \to \infty$ the set of points generated by equation (14) will coincide with y_c.

From equation (15), we can see that as the abscissa x_B varies within the range $[0,\sigma_1/2]$, the corresponding abscissa x_c from the contact point y_c will vary within the range $[0,(\sigma_1 + \sigma_2\cos\gamma)/2]$.

To exemplify this numerical procedure, in figure 9, we show some curves $y_c(\gamma,\sigma_1,\sigma_2,x)$ obtained for different values of γ and $\sigma_1 = \sigma_2$. The corresponding areas $\mathcal{S}_\perp(\sigma,\gamma)$ obtained through numerical integration of the curves y_c, according to equation (12), are reported in table 3. From the figure 8, we could see that for the specific cases $\gamma = 0$ and $\pi/2$, the envelope $y_c(\sigma_1,\sigma_2,\gamma,x)$ must be given by

$$y_c(\sigma_1, \sigma_2, 0, x) = \sqrt{\left(\frac{\sigma_1 + \sigma_2}{2}\right)^2 - x^2} \tag{16}$$

and

$$y_c(\sigma_1, \sigma_2, \pi/2, x) = \frac{\sigma_2}{2} + \sqrt{\left(\frac{\sigma_1}{2}\right)^2 - x^2}, \tag{17}$$

respectivelly. For these cases, equations (16) and (17) enable the analytical solution of equation (12), obtaining $\mathcal{S}_\perp(\sigma,0) = \pi\sigma^2$ and $\mathcal{S}_\perp(\sigma,\pi/2) = (1 + (\pi/4))\sigma^2$, results that agree with the numerical values reported in table 3. Finally, using equation (11) and the results reported in table 3, we can evaluate the excluded volume $v_{ex_{CD}}(\mathcal{A}, \sigma, \gamma)$, that is also shown in figure 3.

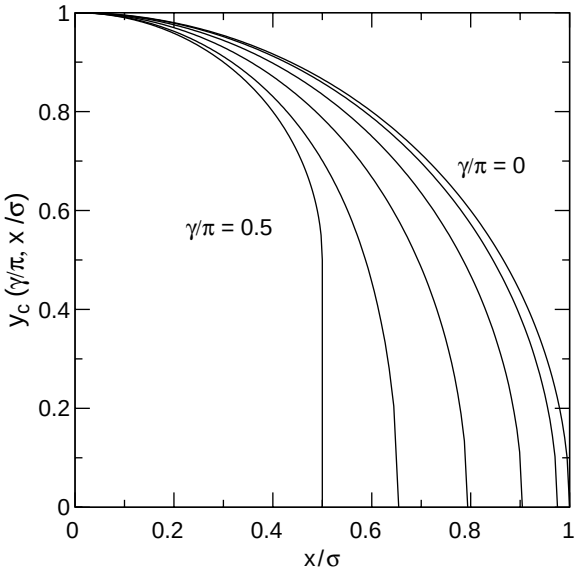

Figure 9. Projections onto the xy-plane of the excluded volume of a cylinder and a disk with the same diameters, $y_c(\gamma,\sigma_1,\sigma_2,x)$. Results were obtained numerically for different values of γ. The curves correspond, from right to left, to the following values of γ/π: 0, 0.1, 0.2, 0.3, 0.4 and 0.5.

Table 3. Area $\mathcal{S}_\perp$ of the transverse projection of $v_{ex_{DD}}$ and $v_{ex_{CD}}$ as a function of the relative orientation γ between disks of diameters $\sigma_1 = \sigma_2 = 1$, obtained through numerical integration of the curves y_c, according to equation (12). The value of $\mathcal{S}_\perp(\sigma,\pi/2)$ is given by the limit $\gamma \to \pi/2$ of $\mathcal{S}_\perp(\sigma,\gamma)$.

γ/π	$\mathcal{S}_\perp(\sigma,\gamma)$
0.00	3.1416
0.05	3.1222
0.10	3.0649
0.15	2.9716
0.20	2.8455
0.25	2.6914
0.30	2.5151
0.35	2.3245
0.40	2.1291
0.45	1.9420
0.50	1.7854

As a final test of the procedure outlined here to determine the exclude volume, we have studied the phase diagram of hard cylinders of aspect ratio $\mathcal{A} = 0.2$, using NPT MC computer simulations, see figure 11. In this figure, we include as a comparison the computer simulation results of Veerman and Frenkel [21] for cut hard spheres, for the same aspect ratio The geometry of both systems is very similar for this aspect ratio value. As we can see from the figure, the simulated hard cylinders reproduce the CS behaviour, indicating that the implementation of the overlap procedure, as described in the Appendix, is correct.

4. Conclusions

In this article, we have presented results of the excluded volume of hard cylinders using two different methods: a MC simulation based on an overlap algorithm, explained in the appendix and a semianalytical procedure, that differs from the Onsager's approach in the way in which the projection of the excluded volume for a disk–disk system is obtained. The MC and semianalytical values agree each other within the statistical uncertainy of the simulation values; however, a deviation with respect to Onsager's results is observed for intermediate values of the aspect ratio $\mathcal{A}$. Closed expressions for the excluded volume and second virial coefficient of theses systems are given. These expressions reproduce the MC and semianalytical values and can be of practical value in the theoretical description of phase diagrams of calamitic and discotic liquid crystal systems, using standard molecular theories for liquid crystals [10,12,24–26]. A detailed description of the overlap algorithm for a system of hard cylinder particles with aspect ratio $\mathcal{A}$ has been also discussed.

Acknowledgements

This work was supported under CONACYT grants 2002-C01-41678 and 2003-C03-42439/A-1.N. Ibarra-Avalos acknowledges a PhD scholarship from CONACYT and CONCYTEG, Mexico.

Appendix

Determination of the overlap configurations of two hard cylinders

We are going to consider a system formed by hard cylinders. A cylinder i is characterized by its center-of-mass position $\mathbf{C}_i = (C_{i1}, C_{i2}, C_{i3})$, orientation unit vector $\hat{\mathbf{n}}_i = (n_{i1}, n_{i2}, n_{i3})$ and its aspect ratio $\mathcal{A} = L/\sigma$, where L is the length and σ the diameter of the cylinder. See figure 10.

A.1 Overlap test between two disk surfaces

We firstly determine overlap configurations between disks of different cylinders. Let us take two disks i and j with centers in $\mathbf{D}_i$ and $\mathbf{D}_j$, respectively.

1. Parallel disks, $\hat{\mathbf{n}}_i = \hat{\mathbf{n}}_j$. In this case, the necessary and sufficient conditions for disks i and j to overlap are: firstly, they must lie on the same plane and secondly, have to be enough close to each other, i.e.

$$\hat{\mathbf{n}}_i \cdot (\mathbf{D}_i - \mathbf{D}_j) = 0 \quad \text{and} \quad (\mathbf{D}_i - \mathbf{D}_j) \leq \sigma.$$

2. Non parallel disks, $\hat{\mathbf{n}}_i \neq \hat{\mathbf{n}}_j$. Each disk defines a plane, let Γ be the intersection line between these planes. In order to have overlap between disk surfaces, it is necessary that both disks intersect Γ, i.e. $\mathbf{P}_i$ and $\mathbf{P}_j$, the points over Γ nearest to $\mathbf{D}_i$ and $\mathbf{D}_j$, respectively must satisfy

$$|\mathbf{P}_i - \mathbf{D}_i| \leq \sigma/2 \quad \text{and} \quad |\mathbf{P}_j - \mathbf{D}_j| \leq \sigma/2. \qquad (18)$$

It can be shown, by minimizing $|\mathbf{P}_i - \mathbf{D}_i|$ under the restrictions $(\mathbf{P}_i - \mathbf{D}_i)\cdot\hat{\mathbf{n}}_i = 0$ and $(\mathbf{P}_i - \mathbf{D}_j)\cdot\hat{\mathbf{n}}_j = 0$, that

$$\mathbf{P}_i = \left[(\mathbf{D}_i\cdot\mathbf{N})\mathbf{N} + (\mathbf{D}_i\cdot\mathbf{n}_i)\left(\mathbf{n}_j\times\mathbf{N}\right) - \left(\mathbf{D}_j\cdot\mathbf{n}_j\right)(\mathbf{n}_i\times\mathbf{N})\right]/\mathbf{N}^2$$

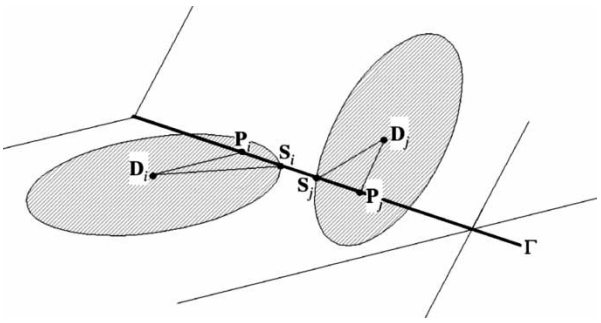

Figure 10. Geometry of disk–disk overlap configurations. Overlap occurs when both disks intersect line Γ and the condition $|\mathbf{P}_i - \mathbf{P}_j| \leq |\mathbf{S}_i - \mathbf{P}_i| + |\mathbf{S}_j - \mathbf{P}_j ?|$ is satisfied.

and similarly,

$$\mathbf{P}_j = \left[\left(\mathbf{D}_j\cdot\mathbf{N}\right)\mathbf{N} + \left(\mathbf{D}_i\cdot\mathbf{n}_i\right)\left(\mathbf{n}_j\times\mathbf{N}\right) - \left(\mathbf{D}_j\cdot\mathbf{n}_j\right)\left(\mathbf{n}_i\times\mathbf{N}\right)\right]/\mathbf{N}^2$$

where $\mathbf{N} = \hat{\mathbf{n}}_i \times \hat{\mathbf{n}}_j$.

If conditions (18) are satisfied, line Γ crosses circumference of disk i at two points $\mathbf{S}_i$ which are simmetrical with respect to **the** line segment $\overline{(\mathbf{D}_i - \mathbf{P}_i)}$; and the same holds for disk j. Clearly (see figure 10) disks overlap if and only if

$$|\mathbf{P}_i - \mathbf{P}_j| \leq |\mathbf{S}_i - \mathbf{P}_i| + |\mathbf{S}_j - \mathbf{P}_j|$$

where the quantities $|\mathbf{S}_i - \mathbf{P}_i|$ and $|\mathbf{S}_j - \mathbf{P}_j|$ are easily calculated as

$$|\mathbf{S}_i - \mathbf{P}_i| = \sqrt{\sigma^2/4 - (\mathbf{P}_i - \mathbf{D}_i)^2}$$

and

$$|\mathbf{S}_j - \mathbf{P}_j| = \sqrt{\sigma^2/4 - (\mathbf{P}_j - \mathbf{D}_j)^2}.$$

A.2 Overlap test of a cylindrical rim and a disk surface

To derive an overlap criterion for this case, let us consider the cylindrical rim of particle i and a disk j. There are many non-overlaping disk–cylinder configurations and is suitable to identify them before doing an overlap test. We denote by $\mathbf{U}_i$ the point in the cylinder axis that is closest to the center of the disk, $\mathbf{U}_i = \mathbf{C}_i + [(\mathbf{D}_j - \mathbf{C}_i)\cdot\hat{\mathbf{n}}_i]\hat{\mathbf{n}}_i$. Then, the overlap between cynlinder and disk does not occur if (a) the sphere that circunscribe the disk does not intersect the cylinder, i.e.

$$|\mathbf{D}_j - \mathbf{U}_i| > \sigma,$$

and (b) if the center of the disk is found in the space zone that corresponds to the extension of the cylinder, i.e.

$$|\mathbf{D}_j - \mathbf{U}_i| < \sigma/2 \quad \text{and} \quad |(\mathbf{D}_j - \mathbf{U}_i)\cdot\hat{\mathbf{n}}_i| > L/2,$$

An overlap between cylinder and disk for this configuration will result neccesarily in a disk–disk overlap, however, this type of configuration has been already discarted. Overlap configurations result when the following two conditions occur,

$$|\mathbf{D}_j - \mathbf{U}_i| \leq \sigma/2 \quad \text{and} \quad |(\mathbf{D}_j - \mathbf{U}_i)\cdot\hat{\mathbf{n}}_i)| > L/2,$$

since in this case the center of a disk is located within the cylinder.

For other relative configurations, the overlap testing can be done by an iterative scheme. Firstly, we will denote by $\mathbf{A}_i$ an arbitrary point on the axis of the cylinder. The nearest point in circumference of disk j to $\mathbf{A}_i$, $\mathbf{T}_j$, is obtained by optimizing $|\mathbf{T}_j - \mathbf{A}_i|$ with the restrictions

$$(\mathbf{T}_j - \mathbf{D}_j)^2 = \sigma^2/4 \quad \text{and} \quad (\mathbf{T}_j - \mathbf{D}_j)\cdot\hat{\mathbf{n}}_j = 0,$$

which yield the two extremal solutions

$$\mathbf{T}_j = \mathbf{D}_j \pm \frac{\sigma}{2}\left[\mathbf{A}_i - \mathbf{D}_j - \left(\left(\mathbf{A}_i - \mathbf{D}_j\right)\cdot\hat{\mathbf{n}}_j\right)\hat{\mathbf{n}}_j\right] / \sqrt{\left(\left(\mathbf{A}_i - \mathbf{D}_j\right)\times\hat{\mathbf{n}}_j\right)^2}. \tag{19}$$

Defining $T_\parallel$ as the projection of $(\mathbf{T}_j - \mathbf{C}_i)$ along $\hat{\mathbf{n}}_i$ and $T_\perp$ as the projection of $(\mathbf{T}_j - \mathbf{C}_i)$ perpendicular to $\hat{\mathbf{n}}_i$ and given that disk–disk overlaps have already been discarded, cylindrical rim and disk overlap if an only if

$$|T_\parallel| \leq L/2 \quad \text{and} \quad |T_\perp| \leq \sigma/2.$$

at least for one of the solutions given by equation (19). In this way, the point in the circumference of the disk that is closest to the cylinder axis is determined iteratively taking $\mathbf{A}_i = \mathbf{C}_i$ and introducing auxiliary vectors $\mathbf{T}_+$ and $\mathbf{T}_-$,

$$\mathbf{T}_+ = \mathbf{D}_j + \frac{\sigma}{2}\left[\mathbf{A}_i - \mathbf{D}_j - \left(\left(\mathbf{A}_i - \mathbf{D}_j\right)\cdot\hat{\mathbf{n}}_j\right)\hat{\mathbf{n}}_j\right] / \sqrt{\left(\left(\mathbf{A}_i - \mathbf{D}_j\right)\times\hat{\mathbf{n}}_j\right)^2},$$

$$\mathbf{T}_- = \mathbf{D}_j - \frac{\sigma}{2}\left[\mathbf{A}_i - \mathbf{D}_j - \left(\left(\mathbf{A}_i - \mathbf{D}_j\right)\cdot\hat{\mathbf{n}}_j\right)\hat{\mathbf{n}}_j\right] / \sqrt{\left(\left(\mathbf{A}_i - \mathbf{D}_j\right)\times\hat{\mathbf{n}}_j\right)^2},$$

The iterative scheme is given by applying the conditions

$$\text{if } T_{-_\perp} < T_{+_\perp} \text{ then } \mathbf{T}_{\text{new}} = \mathbf{T}_-,$$
$$\text{if } T_{+_\perp} < T_{-_\perp} \text{ then } \mathbf{T}_{\text{new}} = \mathbf{T}_+,$$
$$T_{\parallel_{\text{new}}} = (\mathbf{T}_{\text{new}} - \mathbf{C}_i)\cdot\hat{\mathbf{n}}_i, \quad A_i = T_{\parallel_{\text{new}}}\hat{\mathbf{n}}_i + \mathbf{C}_i.$$

In this scheme, we assume that there is a very low probability of finding a configuration which results in $(\mathbf{A}_i - \mathbf{D}_j)\times\hat{\mathbf{n}}_j \equiv 0$. Convergence of $\mathbf{T}_j$ with five significant

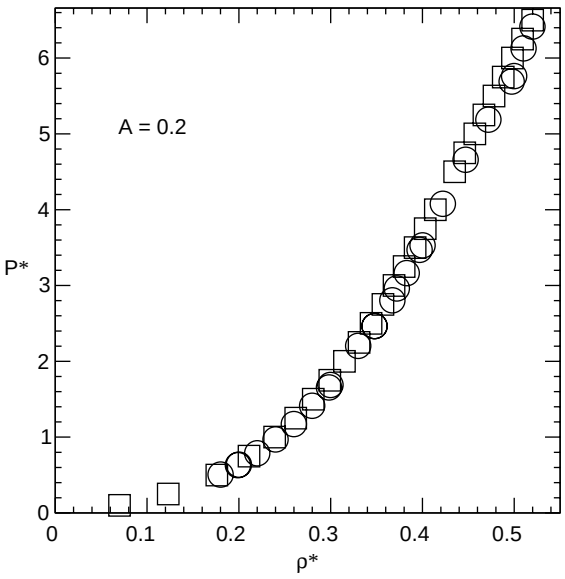

Figure 11. NPT MC computer simulation results for hard cylinders (squares) and CS (circles) for the same aspect ratio, $\mathcal{A} = 0.2$. Pressure ($P^* = Pv_p/kT$, with v_p as the particle volume) is reported as a function of density ($\rho^* = \rho/\rho_0$, where ρ_0 is the crystal's close-packing density). MC Results for the CS system were taken from Ref. [21].

figures is achieved in less than 15 iterations. For most of the studied configurations, no more than eight iterations were required.

A.3 Overlap test of two cylindrical rims

After the former tests are performed, the only kind of possible overlap is between *exclusively* cylindrical rims. Let us introduce the parameters λ_i and λ_j such that the points of closest approach between the lines defined by the axes of the cylinders are

$$\mathbf{V}_i(\lambda_i) = \mathbf{C}_i + \lambda_i \hat{\mathbf{n}}_i$$

for that in line i and

$$\mathbf{V}_j(\lambda_j) = \mathbf{C}_j + \lambda_j \hat{\mathbf{n}}_j$$

for that in line j. The conditions

$$|\mathbf{V}_i - \mathbf{V}_j| \leq \sigma \quad \text{and} \quad |\lambda_i| \leq L/2 \quad \text{and} \quad |\lambda_j| \leq L/2$$

are necessary and sufficient to obtain an overlapping configuration. λ_i and λ_j are obtained by solving the system

$$(\mathbf{V}_i - \mathbf{V}_j)\cdot\hat{\mathbf{n}}_i = 0 \quad (\mathbf{V}_i - \mathbf{V}_j)\cdot\hat{\mathbf{n}}_j = 0$$

explicitly,

$$\lambda_i = \frac{1}{(\hat{\mathbf{n}}_i\cdot\hat{\mathbf{n}}_j)^2 - 1}\left[(\mathbf{C}_i - \mathbf{C}_j)\cdot\hat{\mathbf{n}}_i - ((\mathbf{C}_i - \mathbf{C}_j)\cdot\hat{\mathbf{n}}_j)(\hat{\mathbf{n}}_i\cdot\hat{\mathbf{n}}_j)\right]$$

and

$$\lambda_j = \frac{1}{(\hat{\mathbf{n}}_i\cdot\hat{\mathbf{n}}_j)^2 - 1}\left[(-\mathbf{C}_i - \mathbf{C}_j)\cdot\hat{\mathbf{n}}_j - ((\mathbf{C}_i - \mathbf{C}_j)\cdot\hat{\mathbf{n}}_i)(\hat{\mathbf{n}}_i\cdot\hat{\mathbf{n}}_j)\right]$$

Overlaps between parallel cylinders have been necessarily discarded in overlap tests 1 and 2, then the denominator in the last equations is not equal to zero. So far, we have assumed that the cylinders axes are not collinear. If the axes of two cylinders are colinear overlap exists if an only if $|\mathbf{C}_i - \mathbf{C}_j| \leq L$. The overlap test, we present here is valid for the whole range of aspect ratios. Overlap tests 1 and 2 are crucial for oblate systems, as 2 and 3 are for prolate systems. The test for two cylinders with different aspect ratios can be obtained by a straightforward extension of the procedure described in this section.

References

[1] C.G. Gray, K.E. Gubbins. Theory of molecular fluids. *Volume 1: Fundamentals*, Clarendon Press, Oxford (1984).

[2] W.C.K. Poon, P.N. Pusey. *Observation, Prediction and Simulation of Phase Transition in Complex Fluids*, NATO ASI series C, vol. 460, Kluwer, Dordrecht (1995).

[3] T. Boublik, I. Nezbeda. *P–V–T* behaviour of hard body fluids. Theory and experiments. *Collection Czechoslovak Chem. Commun.*, **51**, 2301 (1986).

[4] M.P. Allen, G.T. Evans, D. Frenkel, B.M. Mulder. *Hard Convex Body Fluids, Advances in Chemical Physics*, vol. LXXXVI, John Wiley & Sons, (1993).

[5] L. Onsager. The effects of shape on the interaction of colloidal particles. *Ann. NY Acad. Sci.*, **51**, 627 (1949).

[6] R. Eppenga, D. Frenkel. Monte Carlo study of the isotropic and nematic phases of infinitely thin hard platelets. *Mol. Phys.*, **52**, 1303 (1984).

[7] D. Frenkel, B. Mulder. The hard ellipsoid-of-revolution fluid I. Monte Carlo simulations. *Mol. Phys.*, **55**, 1171 (1985).

[8] D. Frenkel, H.N. Lekkerkerker, A. Stroobants. Thermodynamic stability of a smectic phase in a system of hard rods. *Nature*, **332**, 822 (1988).

[9] G.J. Vroege, H.N. Lekkerkerker. Phase transitions in lyotropic colloidal and polymer liquid crystals. *Rep. Prog. Phys.*, **55**, 1241 (1992).

[10] S.C. McGrother, D.C. Williamson, G. Jackson. A re-examination of the phase diagram of hard spherocylinders. *J. Chem. Phys.*, **104**, 6755 (1996).

[11] A.G. Vanakaras, D.J. Photinos. Electric dipoles and phase stability in nematic liquid crystals. *Mol. Phys.*, **85**, 1089 (1995).

[12] C. Vega, S. Lago. Isotropic–nematic transition of hard polar and non polar molecules. *J. Chem. Phys.*, **56**, 6727 (1994).

[13] D. Levesque, J.J. Weis, G.J. Zarragoicoechea. Monte Carlo simulation study of mesophase formation in dipolar spherocylinders. *Phys. Rev. E*, **47**, 496 (1993).

[14] D. Levesque, J.J. Weis, G.J. Zarragoicoechea. Singlet orientational distribution function and dielectric permittivity of dipolar spherocylinders in the nematic phase. *Mol. Phys.*, **80**, 1077 (1993).

[15] R. Berardi, S. Orlandi, C. Zannoni. Antiphase structures in polar smectic liquid crystals and their molecular origin. *Chem. Phys. Lett.*, **261**, 357 (1996).

[16] E. de Miguel, E. del Río, J.T. Brown, M.P. Allen. Effect of the attractive interactions on the phase behavior of the Gay–Berne liquid crystal model. *J. Chem. Phys.*, **105**, 4234 (1996).

[17] S.C. McGrother, A. Gil-Villegas, G. Jackson. The effect of dipolar interactions on the liquid crystalline phase transitions of hard spherocylinders with central longitudinal dipoles. *Mol. Phys*, **95**, 657 (1998).

[18] J. Van Duijneveldt, A. Gil-Villegas, G. Jackson, M.P. Allen. Simulation study of the phase behavior of a primitive model for thermotropic liquid crystals: rodlike molecules with terminal dipoles and flexible tails. *J. Chem. Phys.*, **20**, 9092 (2000).

[19] J.W. Perram, M.S. Wertheim. Statistical mechanics of hard ellipsoids. I. Overlap algorithm and the contact function. *J. Comp. Phys.*, **58**, 409 (1985).

[20] R. Blaak, D. Frenkel, B.M. Mulder. Do cylinders exhibit a cubatic phase? *J. Chem. Phys.*, **110**, 11652 (1999).

[21] J.A. Veerman, D. Frenkel. Phase behavior of disklike hard core mesogens. *Phys. Rev. A*, **45**, 5632 (1992).

[22] H. Graf, H. Lowen. Density functional theory for hard spherocylinders: phase transitions in the bulk and in the presence of external fields. *J. Phys. Condens. Matter*, **11**, 1435 (1999). D. Frenkel (1987) "Onsager's spherocylinders revisited", *J. Phys. Chem.*, **91**, 4912-4916; erratum: D. Frenkel (1988) *J. Phys. Chem.*, **92**, 5314.

[23] D.C. Williamson, G. Jackson. Excluded volume for a pair of linear chains of tangent hard spheres with an arbitrary relative orientation. *Mol. Phys.*, **86**, 819 (1995).

[24] S.C. McGrother, R.P. Sear, G. Jackson. The liquid crystalline phase behavior of dimerizing hard spherocylinders. *J. Chem. Phys.*, **106**, 7315 (1997).

[25] E. García, D.C. Williamson, A. Martínez-Richa. Effects of molecular geometry on liquid crystalline phase behaviour: isotropic–nematic transition. *Mol. Phys.*, **98**, 179 (2000).

[26] E. García, A. Martínez-Richa, J.A. Villegas, L.H. Mendoza-Huizar, A. Gil-Villegas. Predicting the phase diagram of a liquid crystal using the convex peg model and the semiempirical PM3 method. *J. Phys. Chem. A*, **106**, 10342 (2002).